Batteries & Supercaps

Research Article
doi.org/10.1002/batt.202200491

Chemistry Europe
European Chemical Societies Publishing

www.batteries-supercaps.org

# On the Reversible Sodium Plating/stripping Reaction in Porous SiCN(O) Ceramic: A Feasibility Study

Marco Melzi d'Eril,*[a] Magdalena Joanna Graczyk-Zajac,*[a, b] and Ralf Riedel[a]

Sodium-ion batteries (SIBs) are a cost-effective and sustainable alternative to lithium-ion batteries (LIBs), which might be independent of rare raw materials. These advantages come at the expense of low energy density. Sodium metal batteries (SMBs) can provide a possible solution. In this work, we present the use of a porous silicon carbonitride (SiCN(O)) ceramic as an anodic matrix for reversible Na-plating. The role of the pores is investigated and the plating mechanism allowing reversible and uniform plating/stripping of sodium is also presented. Electrochemical studies show a stable and reversible capacity gain of around 60 mAh/g beyond the insertion capacity of the SiCN(O) ceramic over 100 cycles.

## Introduction

The concern for a greener and non-oil-reliant future together with the continuous improvement in the fields of the electric automotive industry and renewable energy production act as a driving force for the development of different electrochemical energy storage technologies. The high abundance and low price of sodium make sodium-based batteries one of the potential alternatives to lithium-ion batteries (LIBs) which rely on over-solicited and strongly geographically concentrated reserves of raw materials.[1] Several Na-based technologies such as Na-ion batteries, alloying-metal batteries (including Sb, Sn, and Pb), Na/S, Na/$O_2$, and all-solid-state systems have been deeply investigated.[2–4] Exploiting the LIB expertise would be greatly advantageous. Nevertheless, Na does not form a suitable binary compound with graphite[5] and silicon.[6] This makes the adaptation of the negative electrode from LIBs to Na-based batteries problematic. Yet, considering the astonishing theoretical gravimetric capacity of metallic Na reaching up to 1166 mAh $g^{-1}$ and its high natural abundance, sodium metal batteries (SMBs) seem to be an appealing route. Inspired by the previous work on lithium metallic batteries (LMBs),[7] researchers are seeking solutions[8,9] to overcome the remaining safety and stability issues related to the use of metallic sodium. In recent years, a lot of effort has been made to develop anodeless SMBs. This concept is based on a direct plating/stripping of the metal thus avoiding kinetically slower insertion[10] or alloying processes.[11] In particular, 3D framework current collectors show perspective results and broad application prospects in improving sodium metal anodes.[12] 3D porous materials have been widely studied as functional hosts leading to uniform nucleation based on the interaction between sodium ions and a matrix structure.[9,13] Most studies have attributed porous matrix structures to be beneficial to uniform sodium metallic deposition since pores can induce the initial nucleation by concentrating the ion flux.[14–16] Porous and conductive scaffolds are also expected to simultaneously suppress the Na dendrite growth and minimize the volume changes of Na metal electrodes.[14] Stimulated by this concept, this work presents the first attempt at using a highly porous polymer-derived carbon-rich silicon carbonitride (SiCN(O)) as an anodic matrix for stable and reversible Na-plating/stripping in addition to the storage of Na ions by insertion. Lightweight ceramic materials with a significant amount of a free carbon phase exhibit distinct advantages over porous carbon and metals due to their low mass density, excellent electrical conductivity, and chemical stability rendering them promising host materials for SMB and SIB anodes.[17–21] Ideally, a host should also exhibit good sodiophilicity to facilitate Na metal infusion.[22] In carbon-based materials, the presence of a heteroatom (N, S) in a porous network has been reported to enhance a sodiophilic character and contribute to a homogenous plating morphology with dissipated local current density.[23,24] The investigated carbon-rich porous SiCN(O) provides Na nucleation sites within mesopores making the formation and growth of metallic dendrites unfavorable.

## Results and Discussion

The ceramic has been produced in a porous and non-porous version as explained in the Experimental Section. Henceforth the porous SiCN(O) will be referred to as SiCN(O)-P and the non-porous version as SICN(O)-NP.

Figure 1(a) presents the results of Ar-adsorption/desorption measurements of both porous and non-porous samples. The

[a] M. Melzi d'Eril, Dr.-Ing. M. Joanna Graczyk-Zajac, Prof. Dr. R. Riedel
Department of Material and Earth Sciences
Technical University of Darmstadt
64287 Darmstadt (Germany)
E-mail: marco.melzi@tu-darmstadt.de
graczyk@materials.tu-darmstadt.de
[b] Dr.-Ing. M. Joanna Graczyk-Zajac
EnBW Energie Baden-Württemberg AG
Durlacher Allee 93, 76131 Karlsruhe (Germany)
E-mail: m.graczyk-zajac@enbw.com

Supporting information for this article is available on the WWW under https://doi.org/10.1002/batt.202200491

Research Article
doi.org/10.1002/batt.202200491

Chemistry Europe
European Chemical Societies Publishing

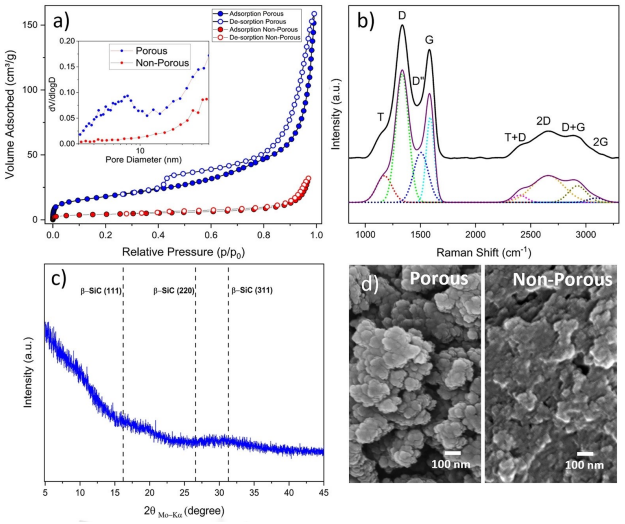


**Figure 1.** a) Physisorption isotherms of the SiCN(O)-P (blue) and SiCN(O)-NP (red) samples and pore size distribution. b) Raman spectrum of the pristine porous material and deconvolution of the bands and their overtones. c) XRD pattern of the pristine porous SiCN(O) and peak position of β-SiC. d) SEM image of the porous (left) and non-porous (right) SiCN(O) acquired at 100k magnification.

blue curve shows a strong increase of the adsorbed volume at a high relative pressure suggesting a type IV adsorption isotherm. This indicates the presence of macropores (also proven by the BJH pore size distribution, see insert in Figure 1a). The hysteresis loop in the relative pressure range from 0.4–0.8 $p/p_0$ originates from the presence of additional mesoporosity. Smaller micropores might be present in the material as well as indicated by the step in the argon uptake at the lowest relative pressures.[25] The calculated SSA of the porous material equals 57 $m^2 g^{-1}$. The isotherm of the SiCN(O)-NP (red curve) suggests a type II isotherm typical for non-porous or microporous materials. The BJH pore size distribution confirms the absence of micro and mesopores. The SSA reaches the value of 13 $m^2 g^{-1}$ which can be induced by the presence of intergranular volume, and therefore the sample can be considered as non-porous. Raman spectroscopy reveals the presence of in-situ formed carbon and shows its characteristic D- and G-band (1350 $cm^{-1}$ and 1582 $cm^{-1}$ respectively) as well as the 2D band at 2700 $cm^{-1}$ and the corresponding overtones (T + D, D + G, and 2G) as shown in Figure 1(b).[26–28] This feature indicates the presence of a free carbon phase embedded within the SiCN(O) mixed-bond phase.[29] The Gaussian fitting applied to the spectrum allows to compare the intensities of the peaks. Using Equation (1) the crystallite size can be calculated.[30]

$$L_a = (2{,}4 \cdot 10^{-10})\ \lambda_l^4 \left(\frac{I(A_D)}{I(A_G)}\right)^{-1} \quad (1)$$

This provides a value of $L_a$ equal to 8.79 nm, which points out the disordered nature of the free carbon.[31] Further, the D''-band (1500 $cm^{-1}$) and the T-band (~1200 $cm^{-1}$) appear in the Raman spectra of materials containing edges or non-planar areas in graphene layers, $sp^3$ hybridization of carbon or pores.[29] Figure S1 in the supplementary data reports the Raman spectra of the SiCN(O)-NP.

The absence of sharp reflections in the XRD pattern (which appear in SiCN(O) with the formation of β-SiC beyond 1400 °C pyrolysis temperature[29]) displayed in Figure 1(c) confirms the disordered structure of free carbon and ceramic phase.[32] The elemental analysis and EDX data reported in Table 1 and Table 2 provide a qualitative overview of the chemical composition of the samples. The unexpected oxygen content of the samples has to be attributed to the instability of the SiCN in air. Exposing this material to the air allows the oxygen to partially replace the nitrogen in the matrix.

Cyclic voltamperommetry measurement (Figure 2a) has been performed to determine the redox potential in a half cell in which the SiCN(O)-P ceramic was cycled against a piece of metallic sodium. During the first voltamperometric reduction cycle in a SiCN(O)-P/$NaPF_6$/Na cell, a cathodic peak is registered at a potential of approximately 0.014 V and correlated to the anodic peak appearing at around 0.12 V. This redox couple is attributed to a reversible insertion/extraction of sodium ions. While extending the potential range to −0.03 V, an additional cathodic peak is detected at around −0.03 V revealing the formation of a metallic Na species whose presence has been recently confirmed employing "in-situ" NMR measurement by Šić et al.[33] The corresponding anodic peak is superimposed with the anodic sodium ion extraction leading to a slightly shifted peak at 0.11 V. To determine the amount of capacity originating from sodium insertion into the porous SiCN(O), a galvanostatic measurement in a range between 0.005 V and 2.5 V has been performed (Figure 2c). An insertion/extraction capacity equal to 340 mAh $g^{-1}$ and 113 mAh $g^{-1}$ respectively

**Table 1.** Elemental analysis of SiCN(O)-P.

| Sample | Composition [wt.%] | | | | Free Carbon [wt.%] | Empirical Formula |
|---|---|---|---|---|---|---|
| | C | O | N | Si | | |
| SiCN(O)-P | 49.4 | 6.5 | 11.0 | 33.1 | 44.8 | $Si_{1.00}C_{3.48}N_{0.66}(O_{0.34})$ |

**Table 2.** EDX analysis of SiCN(O)-P and SICN(O)-NP.

| Sample | Composition [wt.%] | | | | Free Carbon [wt.%] | Empirical Formula |
|---|---|---|---|---|---|---|
| | C | O | N | Si | | |
| SiCN(O)-NP | 53.1 | 6.1 | 8.9 | 32 | 47.4 | $Si_{1.00}C_{3.87}N_{0.55}(O_{0.33})$ |
| SiCN(O)-P | 50.6 | 6.4 | 10.7 | 32.3 | 46.1 | $Si_{1.00}C_{3.65}N_{0.66}(O_{0.34})$ |

Research Article
doi.org/10.1002/batt.202200491

Chemistry Europe
European Chemical Societies Publishing

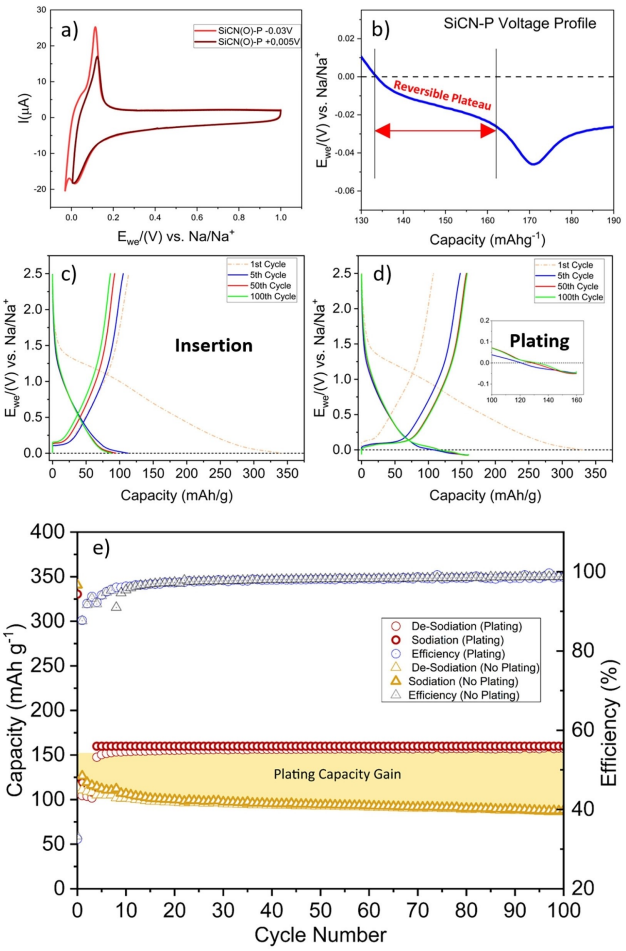


**Figure 2.** a) Cyclic voltammetry in the insertion and plating voltage range. b) Voltage profile inset showing the reversible plateau followed by a pronounced activation peak c, d) Voltage profile of the cell cycled for 100 cycles in the insertion range (c) and in the plating range (d). e) Capacity retention plot showing the capacity gain originating from the plating (yellow area).

has been measured in the first cycle. The following 100 cycles revealed an average capacity of around 94.7 mAh g$^{-1}$ with a maximal Coulombic efficiency of 98.9%. The low capacity retention in the first cycle can be explained with the formation of the SEI on the porous matrix and with a partially irreversible first insertion. By extending the potential limit of galvanostatic cycling to a negative limit, plating becomes part of the electrochemical process. Nevertheless, to allow an organized formation of the SEI, the initial five cycles were carried out limiting the potential range to the positive region (2.5 V/ 0.005 V). Finding a proper negative voltage limit for reversible plating represented a non-trivial task. Preliminary measurements revealed that setting a fixed desired negative voltage value of −0.03 V and plating time is not effective since the overpotential might rise throughout the cycling, shifting the operational range and thus progressively decreasing the capacity gain originated from the plating (Figure S2). Setting the limit intentionally lower in order to give a margin to the system to compensate the overpotential showed the appearance of two plateaus, one in the range between 0 V and −0.04 V and a second one after a pronounced peak at −0.05 V as visible in Figure 2(b). Pushing the system beyond this peak would lead to the formation of a plated species, which is only partially reversible thus dramatically reducing the Coulombic efficiency. For this purpose, the lowest voltage limit was set at −0.15 V but a capacity limitation of 160 mAh g$^{-1}$ was imposed during cycling. This restricted the operational voltage between 2.5 V and a value close to −0.04 V, allowing to hold the system in a sort of reversible plating state. The "plating"-cell has been tested using the setting explained above and the first sodiation capacity reached 342 mAh g$^{-1}$, of which 112 mAh g$^{-1}$ could be reversibly de-sodiated. After the initial five limited cycles (without plating), the cell showed a stable limited capacity of 160 mAh g$^{-1}$ for 100 cycles with a maximal Coulombic efficiency of 98.8% (Figure 2d). The yellow field marked in Figure 2(e) emphasizes the amount of additional capacity which is obtained thanks to a reversible plating. To confirm the functionality of the pores during the electrochemical plating of Na the SiCN(O)-NP previously mentioned has also been tested under the same conditions as for the porous one for a comparison. As visible in Figure 3(a, red line), the galvanostatic reduction curve of the SiCN(O)-NP does not show a plateau in the region prior to the nucleation peak and the reaction takes place at a lower potential. This signifies that the porous supports provide nucleation spots, which are energetically more favorable for sodium deposition. Further, the insertion capacity in the non-porous material is approximately 20% lower. This points out that the presence of the pores not only plays a beneficial role during the plating/stripping process acting as a host site for reversible plating, but also provides additional insertion capacity.

The short plateau recorded before the activation peak is rationalized as follows: until the peak is reached, the plating takes place in the pores of SiCN(O)-P ceramic, providing a highly reversible additional capacity. Once all the available porous sites are occupied, the plating takes place on the surface of the electrode, leading to the formation of partially reversible dendritic sodium islands plated on the electrode surface (compare inserts in Figure 3c) and lowering the Coulombic Efficiency to around 93%. For this reason, the imposed capacity limitation plays a crucial role. If non-porous support is used, plating takes place exclusively at the surface as depicted schematically in Figure 3(c) and the process covers the electrode irreversibly with Na within a few cycles.

Figure 3(b) shows a strong difference in the reversibility of the plating processes. Starting from the top, the electrode kept in the reversible region does not display any Na-metal accumulation on the surface after 100 cycles. Pushing the system beyond the nucleation peak results in the formation of metallic Na clusters on the surface permanently damaging the cell after 70 cycles. The irreversibility of the process becomes even more evident in the non-porous sample which is almost completely covered with metallic Na within less than 30 cycles. Overall, although the capacity retention in the first cycle in both cases is not astonishing as displayed in Figure 2(c and d), the PDC exhibited excellent cycling stability for at least 100 cycles whether during insertion or plating. Methods such

Research Article
doi.org/10.1002/batt.202200491
Chemistry Europe
European Chemical Societies Publishing

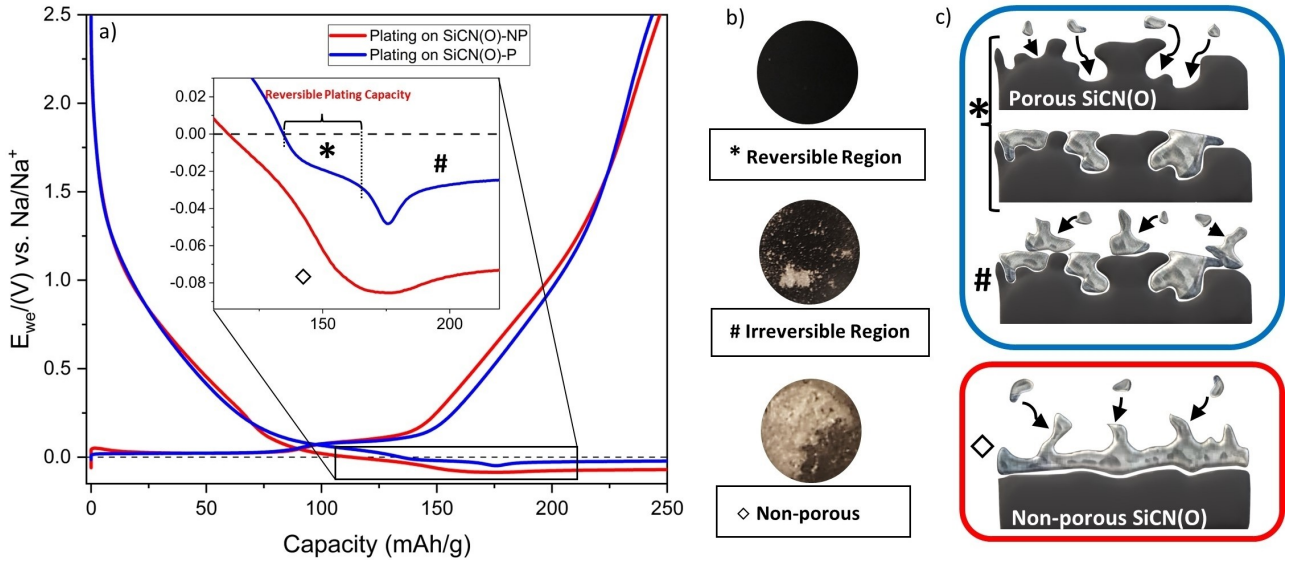


**Figure 3.** a) The figure shows the comparison between the charge/discharge curve (V vs. capacity) of the porous and the non-porous material. The inset on the left shows the reversible plating plateau (blue line) preceding the Na-dendrites nucleation peak. The red line displays the direct formation of irreversible Na on the SiCN(O)-NP. b) The effect of the plating on the electrodes. c) The possible plating mechanism on both types of materials.

as in-situ Scanning Electron Microscopy and Wide and Small Angle X-ray Scattering will be applied in our future studies to investigate the mechanism of plating in detail in order to gain a deeper understanding of the deposition of the sodium in the matrix.[34,35]

## Conclusion

The present study addresses the suitability of polymer-derived porous SiCN(O) matrix as support for sodium plating in Na-metal batteries. Electrochemical tests proved the stability and cyclability of the material for 100 cycles in a half-cell configuration. The role of the pores has been investigated pointing out their function during insertion and plating process. A possible plating mechanism is also proposed. The obtained results build the foundations for further optimization of the process, e.g., by tuning the porosity in order to benefit from an enhanced reversible plating range. The knowledge of plating-based technology will contribute to the further development of efficient and high-energy storage devices in the future.

## Experimental

Hydrosilylation of 33.75 g of perhydropolysilazane (PHPS wt.−20% in di-n-butyl ether, DBE, Merck) was performed by adding 19.52 g of divinylbenzene[36] (DVB, Sigma–Aldrich, UK) to the solution as a cross-linking agent in the presence of 0.06 mL of Pt-catalyst (Pt(0)-1,3-divinyl-1,1,3,3tetramethyldisiloxane, diluted in xylene, Sigma–Aldrich, UK) in a glove box under Ar atmosphere. The solution is stirred for 6 hours at 120 °C under Ar using a Schlenk line. The pre-ceramic is then heated up to 250 °C for 3 hours in a quartz tube to enhance the cross-linking and subsequently pyrolyzed at 1000 °C under constant Ar flow. The porous ceramic material resulting from the heat treatment is ground by hand and subsequently ball-milled down to 40 μm. To investigate the functionality of the pores, the same SiCN(O) material has been also produced in a non-porous version by removing the DBE under vacuum from the polymer, preceding the start of the synthesis.

To confirm the presence of pores, gas adsorption/desorption measurements were carried out. The samples were dried for 16 hours at 100 °C under vacuum and the isotherms have been measured using a 3P-micro300 (3P Instruments, Germany) and Ar at 87 K as adsorbate. The specific surface area (SSA) was calculated using the BET theory. The pore size distribution has been subsequently calculated using the BJH method. Hg-porosimetry has also been measured using a Quantachrome POREMASTER 60-GT. An additional powerful tool for the characterization of this ceramic is the Raman spectroscopy which served to investigate the presence and the morphology of the free carbon in the SiCN(O) matrix. A Horiba HR800 spectrometer was used with a laser wavelength of 514.5 nm (Cobolt Fandango 100 mW) in a wavelength shift range between 0 and 4000 cm$^{-1}$. X-Rays diffractograms were measured using a STOE STAD1 P diffractometer (STOE & Cia GmbH, Germany) equipped with monochromatic Mo–Kα radiation ($\lambda = 0.07093$ nm).

Scanning Electron Microscopy (SEM) micrographs and Energy Dispersive X-Ray analysis (EDX) were acquired for both sample types with a JEOL JSM 7600F equipped with a Schottky emitter. Elemental analysis of the sample SiCN(O)-P was carried out with two different devices. The total carbon content was determined by combustion analysis using a carbon analyzer Leco C-200 (Leco Corporation, Michigan, USA) whereas the oxygen and nitrogen content were measured by hot gas extraction using a N/O analyzer, Leco TC-436 (Leco Corporation, Michigan, USA). The Silicon amount was calculated as the remaining fraction. Testing the electrochemical properties of SiCN(O) required the production of a slurry. 1 g of SiCN(O) powder was mixed with 21.27 mg of carbon black (Super C65, IMERYS) to enhance the conductivity. The binder was obtained by dissolving 21.27 mg of carboxymethylcellulose (CMC, Sigma–Aldrich, UK) in water (wt.−5%). The mechanical stability of the slurry was enhanced with the addition of 53.19 mg of a wt.−40% solution of styrene-butadiene rubber (ZEON, Japan) in water and ethanol. The mixture was then stirred homogeneously

and printed on a copper foil (99,8%, Alfa Aesar) using a doctor blade. The electrodes were electrochemically tested in a half-cell configuration using Swagelok-type cells assembled in a glovebox under Ar atmosphere. 180 μL of a 1 M solution of $NaPF_6$ dissolved in a 6:4 v/v mixture of ethylene carbonate (EC), and diethyl carbonate (DEC) used as electrolyte were dropped on a glass fiber separator (Whatman GE Healthcare). Eventually, a slice of metallic sodium (99,8%, Alfa Aesar) serving simultaneously as a counter electrode and reference electrode was inserted before closing the cell. All the potentials mentioned are therefore referred to as vs. $Na/Na^+$. The samples have been tested using a VMP3 potentiostat (BioLogic GmbH, France). To gather an essential understanding of the electrochemical processes taking place in a half cell, two cyclic voltammetry scans (CV) have been performed at a scan rate of 10 μV/s respectively between 1 V/0.005 V and 1 V/−0.03 V. These values were chosen with a focus on the comparison between the positive range vs. $Na/Na^+$, where only insertion/intercalation processes are expected, and a value in the negative range, where the sodium plating is foreseeable. Galvanostatic cycling with potential limitation has also been measured in the ranges between 2.5 V/0.005 V and 2.5 V/−0.04 V with a current density equal to 37 $mA\,g^{-1}$. After 100 cycles (when possible) the cells have been opened and a picture of the electrode has been taken.

## Acknowledgements

*The authors would like to thank M.Sc. Laura Feldman for the SEM picture and Dr. Konstantin Schutjajew and Prof. Dr. Martin Oschatz for the constructive discussion concerning the topic of this work. Financial support is gratefully acknowledged by the EU-Project SIMBA (Sodium-Ion and Sodium-Metal Batteries for efficient and sustainable next-generation energy storage – https://simba-h2020.eu/), Grant Number: 963542. Open Access funding enabled and organized by Projekt DEAL.*

## Conflict of Interest

The authors declare no conflict of interest.

## Data Availability Statement

The data that support the findings of this study are available from the corresponding author upon reasonable request.

**Keywords:** anode · battery · ceramics · plating · porous · sodium

[1] C. B. Tabelin, J. Dallas, S. Casanova, T. Pelech, G. Bournival, S. Saydam, I. Canbulat, *Miner. Eng.* **2021**, *163*, e106743.
[2] S.-M. Zheng, Y.-R. Tian, Y.-X. Liu, S. Wang, C.-Q. Hu, B. Wang, K.-M. Wang, *Rare Met.* **2021**, *40*, 272–289.
[3] I. Hasa, S. Mariyappan, D. Saurel, P. Adelhelm, A. Y. Koposov, C. Masquelier, L. Croguennec, M. Casas-Cabanas, *J. Power Sources* **2021**, *482*, e228872.
[4] S. Murugan, S. Niesen, J. Kappler, K. Küster, U. Starke, M. R. Buchmeiser, *Batteries & Supercaps* **2021**, *4*, 1636–1646.
[5] H. Moriwake, A. Kuwabara, C. A. J. Fisher, Y. Ikuhara, *RSC Adv.* **2017**, *7*, 36550–36554.
[6] S. C. Jung, D. S. Jung, J. W. Choi, Y.-K. Han, *J. Phys. Chem. Lett.* **2014**, *5*, 1283–1288.
[7] A. Varzi, K. Thanner, R. Scipioni, D. Di Lecce, J. Hassoun, S. Dörfler, H. Altheus, S. Kaskel, C. Prehal, S. A. Freunberger, *J. Power Sources* **2020**, *480*, e228803.
[8] A. P. Cohn, N. Muralidharan, R. Carter, K. Share, C. L. Pint, *Nano Lett.* **2017**, *17*, 1296–1301.
[9] Y. Lu, Q. Zhang, M. Han, J. Chen, *Chem. Commun. (Camb.)* **2017**, *53*, 12910–12913.
[10] V. Surendran, R. K. Hema, M. S. O. Hassan, V. Vijayan, M. M. Shaijumon, *Batteries & Supercaps* **2022**, 5, e202200316.
[11] A. Willow, H. E. M. Hussein, S. Vajirakaphan, A. Chasri, S. Margadonna, *Front. Energy Res.* **2022**, *10*, e888321.
[12] L. Zhang, Y. Xia, H. Yang, S. Xiao, J. Zhou, Y. Cao, T. Qian, *APL Mater.* **2022**, *10*, 70901.
[13] W. Luo, Y. Zhang, S. Xu, J. Dai, E. Hitz, Y. Li, C. Yang, C. Chen, B. Liu, L. Hu, *Nano Lett.* **2017**, *17*, 3792–3797.
[14] B. Sun, P. Li, J. Zhang, D. Wang, P. Munroe, C. Wang, P. H. L. Notten, G. Wang, *Adv. Mater.* **2018**, *30*, e1801334.
[15] Z. Xu, Z. Guo, R. Madhu, F. Xie, R. Chen, J. Wang, M. Tebyetekerwa, Y.-S. Hu, M.-M. Titirici, *Energy Environ. Sci.* **2021**, *14*, 6381–6393.
[16] C. B. Soni, V. Kumar, Z. W. Seh, *Batteries & Supercaps* **2022**, *5*, e202100207.
[17] X. Dou, D. Buchholz, M. Weinberger, T. Diemant, M. Kaus, S. Indris, R. J. Behm, M. Wohlfahrt-Mehrens, S. Passerini, *Small Methods* **2019**, *3*, 1800177.
[18] C. Chandra, H. S. Cahyadi, S. Alvin, W. Devina, J.-H. Park, W. Chang, K. Y. Chung, S. K. Kwak, J. Kim, *Chem. Mater.* **2020**, *32*, 410–423.
[19] C. Chandra, W. Devina, S. Alvin, J. Kim, *Chem. Eng. J.* **2021**, *404*, 126520.
[20] J. Kaspar, M. Storch, C. Schitco, R. Riedel, M. Graczyk-Zajac, *J. Electrochem. Soc.* **2016**, *163*, 156–162.
[21] P. Colombo, *Science* **2008**, *322*, 381–383.
[22] K. Lee, Y. J. Lee, M. J. Lee, J. Han, J. Lim, K. Ryu, H. Yoon, B.-H. Kim, B. J. Kim, S. W. Lee, *Adv. Mater.* **2022**, *34*, e2109767.
[23] X. Chen, Y.-K. Bai, X. Shen, H.-J. Peng, Q. Zhang, *J. Energy Chem.* **2020**, *51*, 1–6.
[24] X. Zheng, P. Li, Z. Cao, W. Luo, F. Sun, Z. Wang, B. Ding, G. Wang, Y. Huang, *Small* **2019**, *15*, e1902688.
[25] M. Thommes, K. Kaneko, A. V. Neimark, J. P. Olivier, F. Rodriguez-Reinoso, J. Rouquerol, K. S. Sing, *Pure Appl. Chem.* **2015**, *87*, 1051–1069.
[26] M. Pawlyta, J.-N. Rouzaud, S. Duber, *Carbon* **2015**, *84*, 479–490.
[27] A. C. Ferrari, J. Robertson, *Phys. Rev. B* **2000**, *61*, 14095–14107.
[28] C. Hu, S. Sedghi, A. Silvestre-Albero, G. G. Andersson, A. Sharma, P. Pendleton, F. Rodríguez-Reinoso, K. Kaneko, M. J. Biggs, *Carbon* **2015**, *85*, 147–158.
[29] G. Mera, A. Navrotsky, S. Sen, H.-J. Kleebe, R. Riedel, *J. Mater. Chem.* **2013**, *1*, 3826.
[30] L. G. Cançado, K. Takai, T. Enoki, M. Endo, Y. A. Kim, H. Mizusaki, A. Jorio, L. N. Coelho, R. Magalhães-Paniago, M. A. Pimenta, *Appl. Phys. Lett.* **2006**, *88*, e163106.
[31] P. Colombo, G. Mera, R. Riedel, G. D. Sorarù, *J. Am. Ceram. Soc.* **2010**, *93*, 1805–1837.
[32] L. M. Reinold, Y. Yamada, M. Graczyk-Zajac, H. Munakata, K. Kanamura, R. Riedel, *J. Power Sources* **2015**, *282*, 409–415.
[33] E. Šić, M. Melzi d'Eril, K. Schutjajew, M. J. Graczyk-Zajac, H. Breitzke, R. Riedel, M. Oschatz, T. Gutmann, G. Buntkowsky, *Batteries & Supercaps* **2022**, *5*, e20220006.
[34] D. Saurel, J. Segalini, M. Jauregui, A. Pendashteh, B. Daffos, P. Simon, M. Casas-Cabanas, *Energy Storage Mater.* **2019**, *21*, 162–173.
[35] T. Tsuda, K. Hosoya, T. Sano, S. Kuwabata, *Electrochim. Acta* **2019**, *319*, 158–163.
[36] D. Vrankovic, M. Storch, C. Schitco, Z. M. Graczyk, R. Riedel (UNIV DARMSTADT TECH [DE]) DE102016116732 (A1), **2016**.

Manuscript received: November 9, 2022
Revised manuscript received: December 21, 2022
Version of record online: January 19, 2023